On the stability of deep-seated landslides. The cases of Vaiont (Italy) and Shuping (Three Gorges Dam, China)

C. Seguí[1], H. Rattez[1], and M. Veveakis[1]

[1]Civil and Environmental Engineering Department, Duke University, Durham, USA.

Corresponding author: Carolina Seguí (carolina.segui@duke.edu)

Abstract

Deep-seated catastrophic landslides are among the most powerful natural hazards on earth. These devastating events are not possible to be prevented yet, because of their large volumes and sudden acceleration phase. The present study suggests a new method to detect when a landslide will turn unstable, giving both a time-window to evacuate the area that is going to be affected and critical values for measurable variables (velocity and basal temperature) up to which remediation measures can be deployed. This work focuses on large ancient landslides reactivated due to human interaction, like the construction of a dam in the vicinity of the landslide that causes water table variations and affects the stability of the landslide. The main hypothesis of this work is that most of the deformation of deep-seated landslides is concentrated on a thin, basal shear band forming the sliding surface. That allows deep-seated landslides to be approximated as elastic/rigid blocks sliding over a visco-plastic shear band, featuring weak phases like expansive clays. When the landslide creeps, it causes friction in the shear band that raises the temperature of the clays until they become unstable and collapse catastrophically through a thermal runaway instability. This study deploys an energy-based approach, accounting for the heat generated due to friction, to find the critical point where the landslide turns unstable. The model is applied to the Vaiont landslide in Northern Italy and the Shuping landslide next to the Three Gorges Dam in China. The results of the model reproduce with great accuracy the sliding behavior of both landslides and enable to retrieve or predict the critical point of stability.

Keywords: Creep, Friction, Groundwater, Landslides, Shear Strength, Temperature Effects

1 Introduction

When large deep-seated landslides collapse they are accompanied by catastrophic impact to societies and infrastructures. This kind of landslides usually has large periods (tens of years) of creeping phases until they collapse suddenly without previous warning. Thus, the main question is why after years of moving slowly (cm/year) they blow-up in minutes. Some of these slides are ancient landslides that remained dormant during centuries and because of human interaction (constructions) they got reactivated and collapsed in a short-period of time (from few years to tens of years). Because of these characteristics, deep-seated landslides present a formidable challenge in their failure prediction.

Common points of focus in landslide modeling include the study of *external factors* that would aggravate the stability of a slope. These factors include groundwater variations due to precipitation or dam construction, seismic activity, etc, and are directly changing the loading conditions of the landslide (shear stress) and therefore the factor of safety [*Yu et al., 2017; Wang et al., 2017; Song et al., 2014*]. However, the factor of safety is a static quantity (calculated from the stresses only) and is of restricted validity in a moving landslide. This leads to the necessity of replacing the concept of factor of safety with a real-time assessment tool. Such a tool was suggested by *Saito* [*1965, 1969*], and later generalized by *Voight* [1*988*] to be the inverse velocity over time approach [*Sornette et al., 2004; Helmstetter et al., 2004*]. More recently *Ma et al.* [*2017*] and *Zhao et al.* [*2016*] generalized the inverse velocity further, by proposing forecasting models of a landslide failure by probabilistic models of the displacements and regression of the groundwater data, respectively. These techniques rely on the empirical observation of deep-seated landslides, but nonetheless provide useful insight on the phenomenology of the latest stages of large earth slides. It seems that modeling of landslides should be enriched with *internal factors* of instability, i.e. physical mechanisms that can change the material's properties (strength, friction coefficient) directly and allow the slide to transition from secondary to tertiary creep.

Several studies [eg. *Kilburn and Petley, 2003*] point out that the basal sliding surface (or shear band), as the weakest part of the landslide, is indeed where such *internal factors* of instability would be of major importance, since this is where the kinematics of the landslide are concentrated. Thus, focusing on understanding the behavior of the shear band could allow us to constrain the failure mechanism of a large deep-seated landslide. It is common that these deep-seated landslides have clays in their sliding surface, which frequently exhibit thermal softening behavior in their frictional properties. Thus, when a landslide gets activated it can enter a positive thermal feedback loop, whereby slow movements (cm/year) along a thin (from cm to m) shear band can cause friction in the material of the shear band which increases the temperature of the material and reduces its friction coefficient [*Anderson, 1980; Voight and Faust, 1982; Lachenbrunch, 1980; Mase & Smith, 1984; Vardoulakis, 2002; Rice, 2006*], and so forth. This process can continue up to the point where the friction coefficient decreases uncontrollably due to a thermal runaway instability [*Gruntfest, 1963*], even without any variations of *external factors* like the loading conditions.

Over the years several authors have been researching on such behavior of the shear band and presenting models of its thermo-poro-mechanical response during slip, especially with clays as the material that forms the gouge [*Vardoulakis, 2002*; *Veveakis et al., 2007; Goren and Aharonov, 2007, 2009; Goren et al, 2010*; *Pinyol and Alonso, 2010; Cecinato and Zervos, 2012; Alonso et al., 2016*]. This paper is also part of an attempt to constrain further the combination of *internal factors* changing the material's friction coefficient (thermal softening) and the temporal variations of *external factors* (driving shear stress) because of groundwater movements. Therefore, we generalize the analysis of *Veveakis et al.* [*2007*], taking into account groundwater variations. By doing so, we aim at providing a kinematic (time-dependent) stability criterion that couples the *external* forcing of a landslide with its *internal* response.

For this analysis we consider two case studies: the Vaiont landslide (Italy) and the Shuping landslide (Three Gorges Dam, China). For the Vaiont slide we will study the period of its last two years of movement until its collapse, reproducing the velocity history as provided by *Müller* [*1964, 1968*], while for Shuping we will study the 10-year period of its creeping phase, reproducing the displacement history as given by [*Yin et al, 2016*]. We have chosen these two landslides as characteristic examples of large deep-seated landslides that have been very well documented. The common characteristics that these two large deep-seated landslides share are that: 1) their shear-bands are formed by clays; 2) they are ancient landslides that reactivated upon the construction of a dam in their vicinity. However, their main difference is their response to the reservoir variations; the Vaiont landslide accelerated when the reservoir level increased, but Shuping stabilizes when the reservoir level rises. Therefore, the two landslides seem to have different *internal* response to similar *external* stimulation, allowing for in-depth assessment of the limitations of our approach.

2 Multi-scale model of a deep-seated landslide

In order to model deep-seated landslides, we use a model incorporating three configurations at two different scales, as initially suggested by *Vardoulakis,* [*2002a*] and explained in Figure 1. In particular, we consider: A) a *static configuration*, in which the topography enables us to calculate the groundwater table and therefore the shear stress applied along the sliding surface of the landslide; (B) a *kinematic configuration*, in which the landslide topography is modelled as an equivalent rigid block geometry sliding on a surface. The displacement of the block is calculated from the geometry and the stresses determined in the static configuration; (C) the *shear-band configuration*, in which a smaller scale is considered. The sliding surface of the kinematic configuration is modelled as a sheared infinite layer and the multi-physical phenomena triggered by the friction are taken into account. In this work we will focus on translational landslides (i.e. the kinematic configuration is an infinite plane) and on the thermo-poro-mechanical behavior of the material in the shear-band. In the following paragraphs we explain in more details how each configuration is approached and linked with the others.

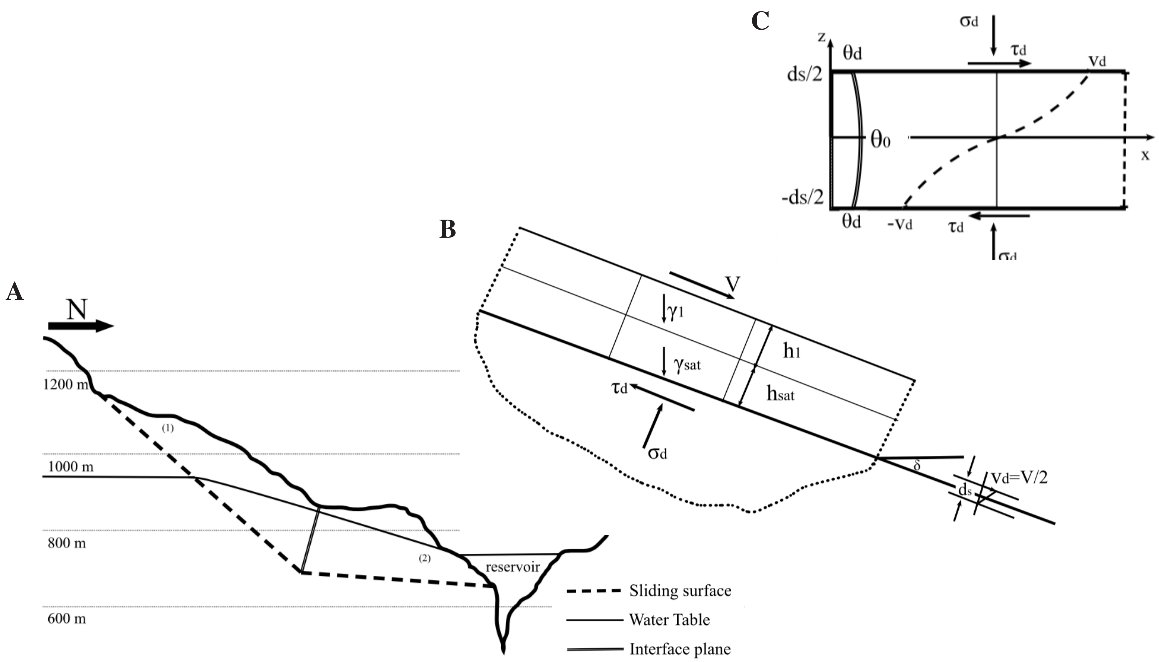

Figure 1. Multi-scale model of a deep-seated landslide. **A)** Static configuration: Topographic cross-section of the landslide in which classical stress calculations are performed. **B)** Kinematic configuration: The landslide is treated as translational, with its kinematics represented as an infinite rigid-elastic block sliding over a shear band. **C)** Shear band configuration: The shear band of the landslide incorporating thermo-mechanical couplings [*Veveakis et al., 2007*].

2.1 Groundwater table of a landslide

We start by calculating the stresses acting along the sliding surface, through a hydro-mechanical analysis of the landslide at the *static configuration* level. For this, we need two elements: the groundwater table and the forces acting inside the landslide. To study the groundwater table of a landslide we use the topographic cross section of the scale (A) in Figure 1 and calculate the hydraulic head (h) at each point of the landslide assuming: 1) horizontal flow, 2) constant Darcy velocity in the horizontal direction, 3) the presence of a free aquifer in the landslide, and 4) that the groundwater discharge is proportional to the saturated aquifer thickness. These assumptions allow us to consider Darcy's law in one dimension as representative of the fluid flow discharge:

$$q = -K\frac{dh}{dl} \tag{1}$$

where q is the specific discharge [m/s], K is the hydraulic conductivity [m/s], $\frac{dh}{dl}$ is the hydraulic gradient, h is the hydraulic head [m], and l is the horizontal characteristic dimension [m].

Considering the above assumptions, the final equation describing the evolution of the water table consists of the mass balance equation, written for the hydraulic head [see *Craig, 2004*]:

$$\frac{\partial h}{\partial t} = D\frac{\partial^2 h}{\partial x^2} \tag{2}$$

where D is the diffusivity [m^2/s], and the hydraulic head is related to the pore fluid pressure P_f [kPa] as $h = \frac{P_f}{\rho g} - z$. Equation (2) is solved analytically, with appropriate boundary conditions,

$$\begin{cases} x = x_1 \rightarrow h = H_1 \\ x = x_2 \rightarrow h = H_2 \end{cases} \tag{3}$$

to obtain:

$$h = \frac{(H_1 - H_2)\,\mathrm{erf}\left(\frac{\xi}{2}\right) + H_2\,\mathrm{erf}\left(\frac{\xi_1}{2}\right) - H_1\,\mathrm{erf}\left(\frac{\xi_2}{2}\right)}{\mathrm{erf}\left(\frac{\xi_1}{2}\right) - \mathrm{erf}\left(\frac{\xi_2}{2}\right)} \tag{4}$$

where $\xi_i = \frac{x_i}{2\sqrt{kt}}$, and *erf* is the error function, $\mathrm{erf}\,(z) = \frac{2}{\sqrt{\pi}}\int_0^z e^{-t^2}dt$. This equation describes the hydraulic head inside the body of the slope, and it can be determined by two values of the hydraulic head (through piezometers or lake elevation) at selected points x_1 and x_2 and the time. In the next section, we use this information to calculate the stresses acting on the sliding surface of a landslide.

2.2 Force equilibrium and Coulomb mechanism of a landslide

Once the groundwater level of the landslide has been evaluated, we can calculate the shear stress of the landslide depending on the groundwater level in the *static-configuration* scale (A) in Figure 1. To this end, the two-wedge method [*Alonso, 1989*] is applied. The forces at equilibrium are calculated separately for each wedge and, then, we calculate the total shear stress of the landslide as the mean of the barycentric shear stresses acting at the bottom of the two blocks [*Alonso and Pinyol, 2010*]. Thus, we divide the landslide into two blocks based on the topography, setting the division line between the point where the interface layer changes the slope at the bottom, and the point where the topography changes the slope drastically at the top (Figure 2). It should be noted that the two-wedge method is just one of the available force equilibrium approaches (others being the Fellenius or Bishop method of slices) and is used here for simplicity in the mathematical treatment.

We consider that the Wedge 1 acts on the Wedge 2 as an active force, and the Wedge 2 acts on the Wedge 1 as a passive force. This consideration has been made taking into account the slopes of the shear band of each wedge. Thus, the wedge that has the higher shear band slope acts actively, and the wedge that has lower shear band slope acts passively.

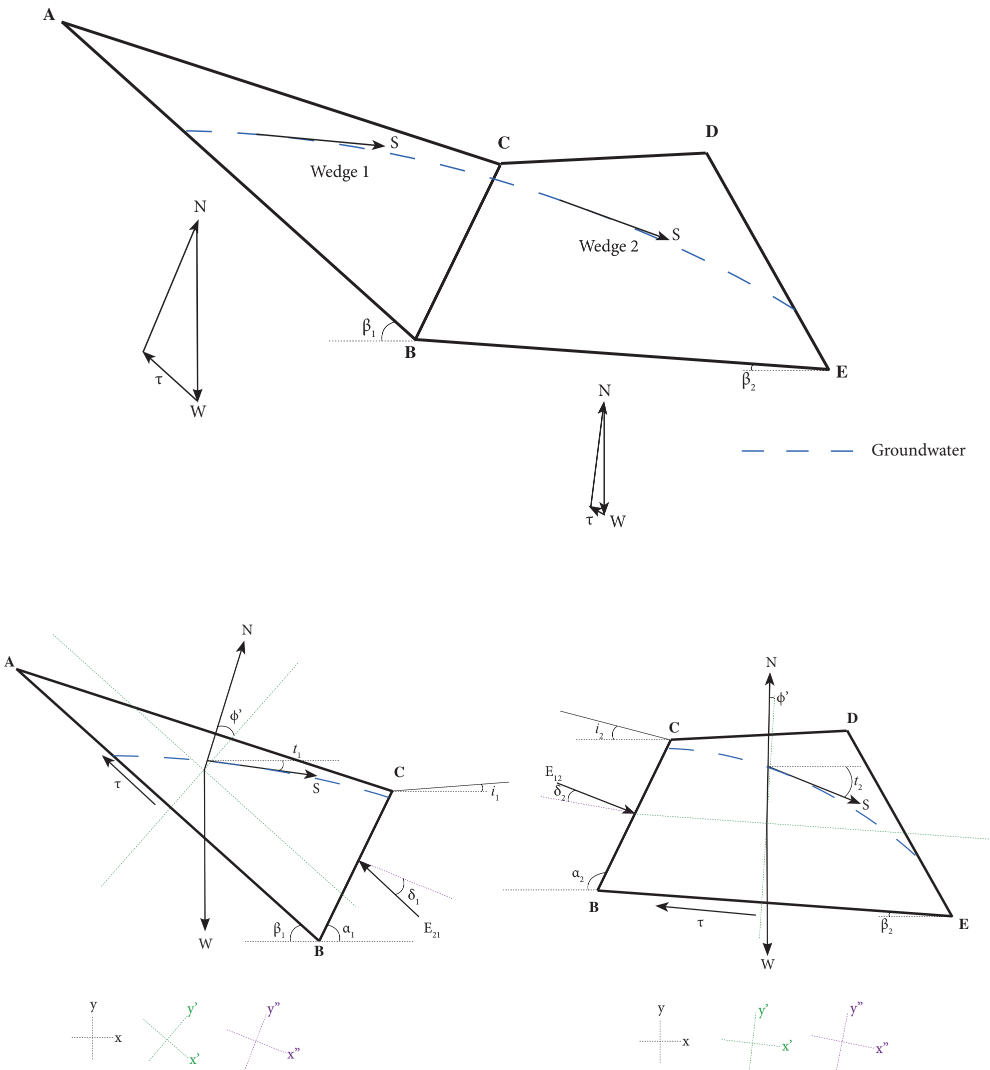

Figure 2. Top: Section profile of a deep-seated landslide with a two-wedge mechanism and its force equilibrium. Bottom: the forces acting on each of the two wedges. Where *N* is the normal force, *S* is the seepage force, *W* is the weight, τ is the shear stress, and E_{12} and E_{21} are the lateral pressures.

The forces acting on Wedge 1 and Wedge 2 are the weight and seepage forces. The weight W [kN] of each wedge is calculated as:

$$W = \gamma_{sat} A_{sat} + \gamma_{dry} A_{dry} \tag{5}$$

where γ_{dry} is the specific unit weight of the soil [kN/m^3], which is the difference between γ_{sat} (specific unit weight of saturated soil [kN/m^3]) and γ_w (specific unit weight of water [kN/m^3]), A_{sat} is the area of saturated soil [m^2], and A_{dry} is the area of dry soil [m^2]. The seepage force S [KN/m] is acting as a positive force on each wedge, and is calculated as:

$$S = A_{sat}\, \gamma_w \tag{6}$$

Applying the earth pressure theory of Rankine [see chapter 11 of *Craig, 2004*], we can calculate the active and passive forces of the landslide as follows. The active force is:

$$E_{12} = \left(0.5\, \gamma_{sat}\, H_{sat}^{\ 2}\, k_a \text{-}\ 2\, c\, H_{sat} \sqrt{k_a}\right) + \left(0.5\, \gamma_{dry}\, H_{dry}^{\ 2}\, k_a \text{-}\ 2\, c\, H_{dry} \sqrt{k_a}\right) \tag{7}$$

where E_{12} is the active earth force [KN] acting in the Wedge 2, H_{sat} and H_{dry} are the normalized heights of saturated soil and dry soil [m] respectively at the interface line between the two wedges, c is the cohesion [KN/m^2], and k_a is the active lateral earth pressure coefficient [-] calculated as follows by Rankine's theory:

$$k_a = \frac{\sin^2(\alpha_1+\phi)}{\sin^2\alpha_1 \sin(\alpha_1\text{-}\delta_2)[1+\sqrt{\frac{\sin(\phi+\delta_2)\sin(\phi\text{-}\beta_2)}{\sin(\alpha_1\text{-}\delta_2)\sin(\alpha_1+\beta_2)}}]} \tag{8}$$

with α_1 being the angle of the interface line that divides the two blocks with the horizontal [°], ϕ the friction angle [°], δ_2 [°] is set at 2/3 of the friction angle [*Craig, 2004*], and β_2 the angle of the topography of the Wedge 2 against the horizontal [°].

The passive earth force E_{21} [KN] acting in the Wedge 1 is:

$$E_{21} = \left(0.5\, \gamma_{sat}\, H_{sat}^{\ 2}\, k_p \text{ - } 2\, c\, H_{sat} \sqrt{k_p}\right) + \left(0.5\, \gamma_{dry}\, H_{dry}^{\ 2}\, k_p \text{ - } 2\, c\, H_{dry} \sqrt{k_p}\right) \tag{9}$$

where k_p is the passive lateral earth pressure coefficient [-], calculated as follows by Rankine's theory:

$$k_p = \frac{\sin^2(\alpha_2\text{-}\phi)}{\sin^2\alpha_2 \sin(\alpha_2+\delta_1)[1\text{-}\sqrt{\frac{\sin(\phi+\delta_1)\sin(\phi+\beta_1)}{\sin(\alpha_2+\delta_1)\sin(\alpha_2+\beta_1)}}]} \tag{10}$$

In this expression, α_2 is calculated as $\alpha_2 = \pi - \alpha_1$, δ_1 [°] is 1/3 of the friction angle [*Craig, 2004*], , and β_1 is the angle of the topography of the Wedge 1 with the horizontal [°].

Thus, the horizontal forces acting on Wedge 1 at equilibrium are as follows:

$$\tau + E_{21_H} \text{ - } S\cos(\beta_2\text{-}\alpha_2) + N\sin(\varphi') \text{ - } W\cos(\beta_2) = 0 \tag{11}$$

where N is the normal force acting on both wedges [KN], τ is the shear stress force [KN] acting at the bottom of the wedge as negative on both wedges, and φ' is the friction angle of the soil [°].

Correspondingly, horizontal force equilibrium for the Wedge 2 reads:

$$\tau \text{ - } E_{12_H} \text{ - } S\cos(\beta_1\text{-}\alpha_1) + N\sin(\varphi') \text{ - } W\cos(\beta_1) = 0 \tag{12}$$

where β_1 is the slope of the shear band of the Wedge 1 with the horizontal [°].

The vertical equilibrium forces acting on Wedge 1 (Equation 13) and on Wedge 2 (Equation 14) are as follows:

$$\mathrm{N}\cos(\varphi') - \mathrm{W}\sin(\beta_2) + \mathrm{S}\sin\left(\beta_2 - \alpha_2\right) + \mathrm{E}_{21_\mathrm{V}} = 0 \tag{13}$$

$$\mathrm{N}\cos(\varphi') - \mathrm{W}\sin(\beta_1) + \mathrm{S}\sin\left(\beta_1 - \alpha_1\right) - \mathrm{E}_{12_\mathrm{V}} = 0 \tag{14}$$

Thus, we calculate the normal (N) and shear (S) forces (as a system of equations) for wedge 1 with Equations 11 and 13, and for wedge 2 with Equations 12 and 14. By then dividing *S* with the length *L* (assuming unit length in the third direction) of the sliding surface, we calculate the mean basal shear stress force for the landslide [*Muller, 1968*] as follows:

$$\bar{\tau}_\mathrm{d} = \frac{1}{\mathrm{h}^{(1)} + \mathrm{h}^{(2)}} \left(\mathrm{h}^{(1)}\tau_\mathrm{d}^{(1)} + \mathrm{h}^{(2)}\tau_\mathrm{d}^{(2)}\right) \tag{15}$$

In this expression, $\bar{\tau}_\mathrm{d}$ is the mean (at the center of mass) shear stress of the landslide [MPa], $\mathrm{h}^{(1)}$ is an average height of dry soil height plus saturated soil height of Wedge 1, $\tau_\mathrm{d}^{(1)}$ is the shear stress of Wedge 1, $\mathrm{h}^{(2)}$ is an average height of dry soil height plus saturated soil height of Wedge 2, and $\tau_\mathrm{d}^{(2)}$ is the shear stress of Wedge 2 .

2.3 Thermo-poro-mechanical behavior of the shear band

After calculating the stresses acting on the landslide, we consider the 1D rigid-block/shear-band configuration. We briefly present the conceptual model used in the paper of *Veveakis et al.* [*2007*] in order to model such a deep-seated landslide, incorporating the *kinematic configuration* and *shear-band configuration* scales, as shown in Figure 1B and 1C. As such, a translational landslide is approached as an infinite rigid-elastic block sliding over a thin layer of clay (i.e. the shear zone). The slope where the infinite rigid-elastic block is sliding, has been considered as a mean between the slopes of the two-wedges of the landslide, so that the dynamics of the landslide is respected [see *Veveakis et al.*, *2007*]. As the block is assumed rigid, the velocity along the direction perpendicular to the sliding surface is constant. The rigid-elastic block therefore admits the shear-stresses calculated in the previous section (2.2) in its center of mass, and because we consider that the contact between the base of the infinite rigid-elastic block and the shear band is continuous, the shear stress is applied on the shear band.

Based on the acceptance that clays reach critical state upon relatively small displacements when sheared [*Tika and Hutchinson*, *1999*], we assume that the clay material inside the shear zone is assumed to be at critical state for every variation of the groundwater table and is, thus, deforming under constant volume. This assumption implies that any volumetric effect is negligible [see *Veveakis and Regenauer-Lieb, 2015*]. The shear zone material is assumed to be always fully saturated with water and the various mechanical fields vary along the z-axis, establishing a single dimension model. The behavior of the clay material in the shear zone is considered to exhibit thermal and rate sensitivity, following the work of *Vardoulakis*, [*2002a*]. We assume velocity hardening, meaning that the strain-rate increases when the shear stress rises, and thermal softening, implying that when the temperature in the clays increases the friction coefficient of the material decreases.

Thus, the friction coefficient at critical state (Equation 16) can be defined as a multiplication between a power law dependency for the velocity and an exponential thermal softening, so that the two effects are competitive and can maintain a constant value of the friction coefficient:

$$\mu_{cs} = g(\dot{\gamma}) \cdot f(\theta) = \mu_{ref} \left(\frac{\dot{\gamma}}{\dot{\gamma}_0}\right)^N e^{-M(\theta-\theta_1)} \quad (16)$$

where μ_{cs} is the critical state friction coefficient, μ_{ref} is the reference friction coefficient, $\dot{\gamma}$ is the shear strain-rate, $\dot{\gamma}_0$ is the reference strain-rate, N is the frictional rate-sensitivity coefficient [-], M is the frictional thermal-sensitivity coefficient [°C^{-1}], θ_1 is the reference temperature [°C], and θ is the actual temperature in the shear band [°C].

Considering that the friction coefficient at critical state is defined as $\mu_{cs} = \frac{\tau}{\sigma_n}$, where τ is the shear stress and σ_n is the normal stress, we assume the shear band material to be perfectly visco-plastic:

$$\dot{\gamma} = \dot{\gamma}_0 \left(\frac{\tau}{\sigma_n}\right)^{1/N} e^{m(\theta-\theta_1)}, \quad m = \frac{M}{N} \quad (17)$$

where m is the exponent ratio of the temperature sensitivity coefficient over the strain rate sensitivity coefficient [°C^{-1}]. Note that the exponential dependency on temperature, shown in Eqs. (16-17), corresponds to the low-temperature approximation of the more generic Arrhenius law, as used in the same mechanical considerations for the mechanics of faults, at deeper (therefore higher temperature) environments than landslides [*Alevizos et al, 2014; Veveakis et al., 2014; Poulet et al, 2014*].

Having established the constitutive law for the basal material, the mathematical model of the shear-band [see *Veveakis et al*., *2007*, for a detailed description] comprises: 1) the heat diffusion equation for local entropy production:

$$\rho C \frac{\partial \theta}{\partial t} = k\nabla^2\theta + \tau\,\dot{\gamma} \quad (18)$$

where ρC is the specific heat of the mixture [J (Kg °C)$^{-1}$], k is the Fourier's thermal conductivity of the clay [cal (°C m s)$^{-1}$], and $\tau\,\dot{\gamma}$ is the rate of heat produced due to plastic dissipation ; and, 2) the momentum balance for clay in one dimensional simple shear for each direction:

X direction: $\frac{\partial \sigma_{xy}}{\partial y} = 0$, thus $\sigma_{xy} = \tau_d$ (19)

Y direction: $\frac{\partial \sigma_{yy}}{\partial y} = 0$, thus $\sigma_{yy} = \sigma_n$ (20)

Equations (17-20) can be combined in a single dimensionless equation. By using the following dimensionless quantities:

$$z^* = \frac{z}{\left(\frac{ds}{2}\right)}, \qquad t^* = \frac{k_m}{\left(\frac{ds}{2}\right)^2} t, \quad \theta^* = m(\theta - \theta_1) \quad (21)$$

we obtain the final, single parameter equation describing the thermo-mechanical response of the basal material::

$$\frac{\partial\theta^*}{\partial t^*}=\frac{\partial^2\theta^*}{\partial z^{*2}}+\mathrm{Gr}\,\mathrm{e}^{\theta^*},\ \ z\in\left[-1,1\right],\ \ t>0 \tag{22}$$

In this expression, the only dimensionless group/parameter, Gr, is the so-called Gruntfest number [*Gruntfest*, *1963*],

$$\mathrm{Gr}=\mathrm{m}\frac{\dot{\gamma}_0}{\mathrm{k_m}}\left(\frac{\mathrm{ds}}{2}\right)^2\sigma_{ref}\left(\frac{\bar{\tau}_\mathrm{d}}{\sigma_{ref}}\right)^{1+1/N}, \tag{23}$$

where $\bar{\tau}_\mathrm{d}$ depends on the lake water level variations. In these equations ds is the real thickness of the shear band [m], z is the vertical axis of the one dimensional model of the shear band from Figure 1C [m], k_m is the thermal diffusivity of the soil-water mixture [m^2/s], and t is time [s].

The Gruntfest number expresses the ratio of the mechanical work converted into heat over the heat diffusion capabilities of the material. It includes all the material properties at hand (thermal conductivity, rate and thermal sensitivities, and reference rate), as well as the thickness of the shear band and the normal and shear stresses applied on it. Since these stresses are calculated in the previous sections and evolve with the groundwater level, *Gr* is not constant in time. Therefore, in our analysis, we include the variations of the shear stress into the Gruntfest number to calculate the evolution of temperature in time.

3 Stability analysis of a deep-seated landslide

Having established the governing equation in the shear band, we need to assess the regions of stability of the system. This is achieved by performing a numerical bifurcation analysis of the steady state of Equation (22),

$$\frac{\partial^2\theta^*}{\partial z^{*2}}+\mathrm{Gr}\,\mathrm{e}^{\theta^*}=0, \tag{24}$$

with respect to the only free parameter of the problem, the Gruntfest number *Gr*. The numerical bifurcation is performed by using a pseudo arc-length continuation approach [*Chan and Keller, 1991*, *Veveakis et al., 2010*].

The results of this analysis are presented in Figure 3A, where the maximum value of the dimensionless temperature solution of the steady state equation (Equation 24) is plotted as a function of the bifurcation parameter *Gr*. We can notice the presence of two steady state solutions for values of the *Gr* lower than its critical value of Gr_c~0.88, one at the turning point (black dot) where Gr = $\mathrm{Gr_c}$, and no steady state solution when Gr > $\mathrm{Gr_c}$. The lower branch is a stable attractor of the transient system, whereas the upper branch is an unstable repeller [see also *Veveakis et al., 2010*]. These results therefore delimit the stable area of our system to be the highlighted grey area of Figure 3A. Should the system be somehow pushed outside this area, a catastrophic infinite increase of the temperature will occur, a response known in the literature as thermal runaway [*Gruntfest, 1963*] or thermal blow-up instability [*Veveakis et al, 2007*].

In order to illustrate this response in terms of both temperature and velocity transient evolution inside the shear band, we select two points as initial conditions of the system (points 1 and 2 in Fig. 3A). If the system is at an initial state represented as point 1, which corresponds to a Gruntfest value below the critical point (Figure 3A), the temperature and velocity of the system tend to a steady value (Figure 3B and 3C). This means that indeed when the Gruntfest number of the landslide is located below the turning point, the slope would be creeping in a stable manner.

However, starting at point 2, corresponding to a Gruntfest value above the critical point (in Figure 3A), the temperature and velocity would increase exponentially (i.e. blow-up) over time (Figure 3B and 3C), leading the landslide to collapse catastrophically in finite time.

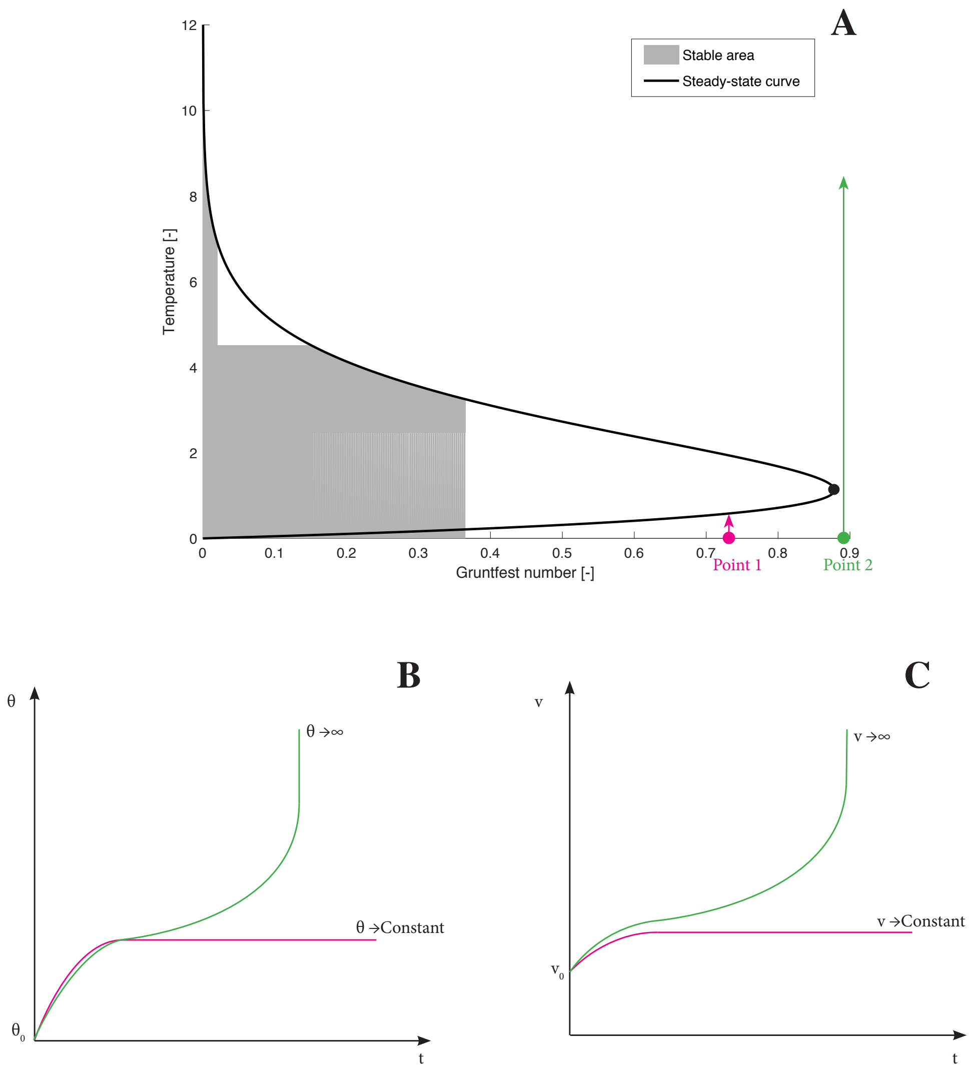

Figure 3. A) Steady-state curve with its critical point (black dot), stable point 1 (pink dot and arrow), and unstable point 2 (green point and arrow). **B)** Representation of the stable and unstable points from Figure 3A in terms of temperature versus time. **C)** Representation of the stable and unstable points from Figure 3A in terms of velocity versus time.

This analysis highlights the crucial role of the Gruntfest number in the stability of the system, suggesting that it is the driving factor for the stability of a landslide. As already discussed, *Gr* is *not* constant over time, as it incorporates the loading conditions (shear stress) of the landslide:

$$Gr = m\,\tau_{(1,1)}\,\dot{\gamma}_0^{\frac{ds^2/4}{k_m}}\,\tau^{1+\frac{1}{N}} \tag{25}$$

Recall that in this expression, τ is the shear stress in dimensionless form, and $\tau_{(1,1)}$ is the initial value of the shear stress.

Using this definition of the Gruntfest number, and the values of the shear stress calculated through our groundwater analysis (Equations 1 to 4), we can determine the stability threshold of a landslide through the bifurcation analysis presented in this section. In the next sections we apply the model to two case studies with different behaviors: 1) the Vaiont landslide in Italy, which turned unstable after years of slow creep and failed catastrophically; and 2) the Shuping landslide in China which has been creeping stably for decades.

4 Case study: Vaiont landslide

The famous Vaiont landslide (Figure 4A and 4B) occurred in October 9th of 1963 in Northern Italy. It has been reported in literature as an ancient landslide that reactivated when the Vaiont dam was built and started filling the reservoir in 1959 [*Semenza and Melidoro, 1992*]. Recent studies [*Dykes and Bromhead, 2018a,b*] suggest that the final catastrophic landslide could be seen as a first time event, in which case the 3 years of creep would only contribute to the landslide progressively losing its structural strength and the dolomite layers to crack forming a weak shear band. Although theoretically possible, such a mechanism cannot be validated or invalidated by current field evidence or existing data collected from the site. As such, in this work we will assume that the landslide is a reactivation, allowing us to set the basal material at critical state and deploy the suggested framework. The validity of this assumption can be tested from the performance of the model against real velocity data for the total 2 years of creep of the landslide.

During the period of three years that the landslide was creeping, the lake level fluctuated depending on the season of the year, from 590 to 710 meters (Figure 4E). Due to the fact that the landslide was instrumented, it had been seen that the velocity of the slide increased when the lake level rose. Therefore, the landslide was stabilized by controlling the lake water level. However, in September 1st of 1963 the lake water level reached 710m and the slide started accelerating, and even though the water level was reduced in October 2nd of 1963 in order to stop the acceleration, the landslide accelerated until it became catastrophic. The average thickness of this slide was about 150 m and had a mass of $2.7\text{x}10^8$ m^3 composed of rocks (Figure 4C). When the event occurred, the rock mass slid into the reservoir creating a wave over 200m height that overflowed the dam and caused 2000 casualties in the downstream valley.

4.1 Geographical location and geological framework

The Vaiont dam is situated in a steep valley in the Italian Alps, located under the Mount Toc in the Pordenone province, region of Friuli-Venice Julia in Northern Italy (Figure 4A). The Piave river was crossing this valley and ending up in the Vaiont Lake. Upstream the river, the valley is wide as it was formed by glacial erosion, and downstream the valley is narrower, which made it an appropriate location for a dam. The stratigraphy of the area (Figure 4D) is composed of massive oolitic calcarenite from the Calcare of Vaiont formation, biocalcarenites and micritic limestone from the Fonzano formation, reddish and grey micrite with ammonites with thin layers of clays from Ammonitico Rosso formation, and intercalations of microcrystalline limestones, calcarenites and loam from the Calcare of Soccher formation of the Lower Cretaceous [*Ferri et al, 2011*].

Due to the fact that the mass of rock was sliding over clay layers, a more detailed information of the clay layers is needed. They are composed of 35 to 80% of a mixture of different types of clays (Ca-montmorillonite, smectite, illite and vermiculite) with grains of calcite and some traces of quartz. These kinds of clays are frequently called "expansive clays" which have a low shear strength and in the presence of water they have a swelling response.

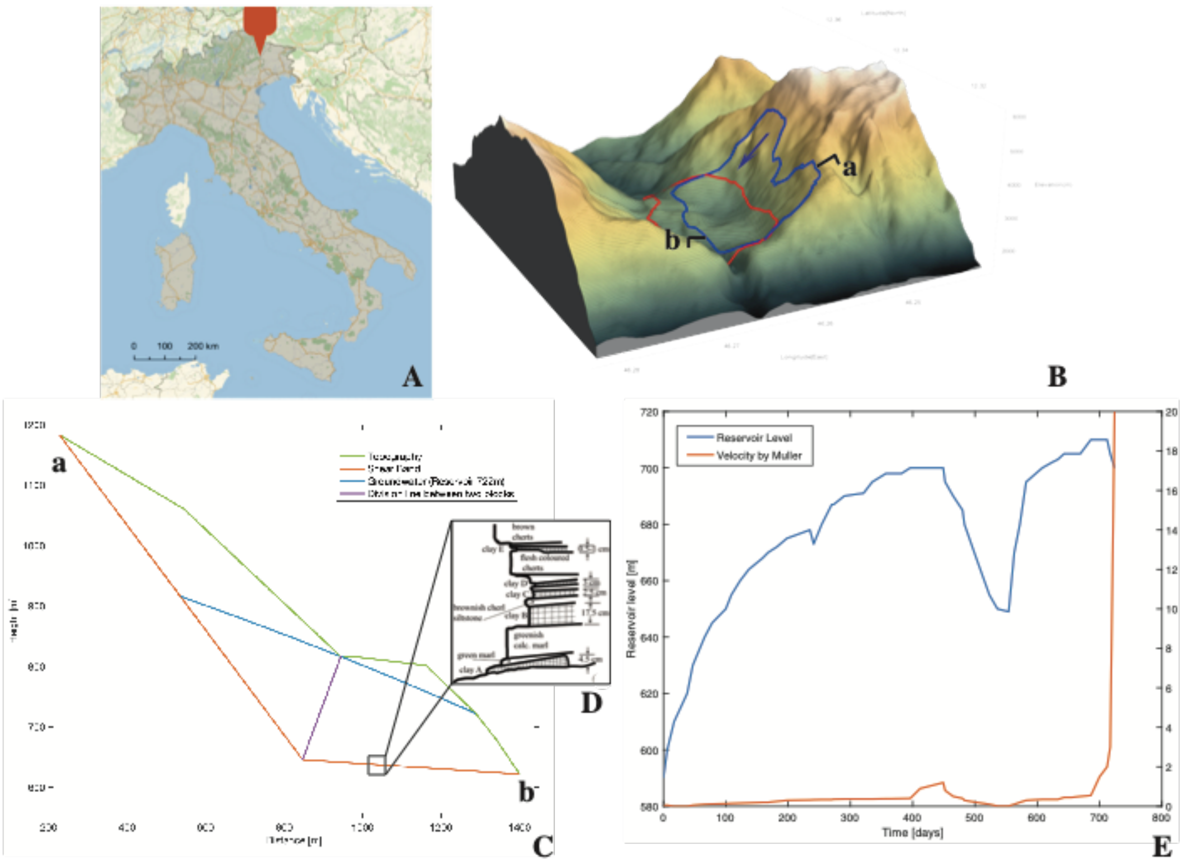

Figure 4. A) Map of location of the Vaiont dam. **B)** 3D elevation map of the Vaiont landslide (blue is the initial position of the mass, and red is the final position of the mass after the collapse). **C)** Profile of the deep-seated Vaiont landslide. **D)** Stratigraphic profile of the lithology of the Vaiont landslide [*Veveakis et al, 2007*]. **E)** Graph showing the reservoir level and the velocity of the landslide during the last two years of recording data [*Muller1964, 1968*].

4.2 Groundwater analysis

The groundwater table of the Vaiont landslide has been calculated considering that the dolomite is permeable enough to allow the groundwater to reach steady state in between the lake level variations. Thus, we calculate the groundwater level by setting Equation (2) to steady state, therefore retrieving the Dupuit-Forchheimer parabola:

$$h=\sqrt{H_1^2-(H_1^2-H_2^2)\frac{x}{L}} \tag{26}$$

where h is the height of groundwater , H_1 is the height of water level of the reservoir, H_2 is the height of groundwater at the fixed point in the back of the landslide, L is the horizontal length between the point of reservoir in contact with the topography of the landslide and the fixed point in the back of the landslide, and x is the horizontal coordinate of a point between the two reference points of water level.

4.3 Shear stress results

Due to the lack of acceptable data for the piezometers [see *Hendron and Patton, 1985* for a comprehensive discussion on this topic], the underground water level is assumed to be always at the maximum level, overestimating the mean basal shear stress by ~0.1 MPa during the periods of low precipitation and snowmelt. From the computed reaction forces at the bottom of the rock mass, the mean values for the shear and normal effective stresses are calculated. Following the double wedge procedure described in section 2.2, and using the lake level data of Figure 4E, a linear dependency between the lake level and the geostatic shear stresses is obtained. This linear dependency is due to the mass of the slide behaves as a free aquifer and has a high permeability; thus, the groundwater level behaves as the reservoir level.

$$\tau = 0.0017\ \mathrm{hl} - 0.118 \tag{27}$$

where τ is the shear stress in MPa, and hl is the reservoir level in meters.

Thus, Figure 5A shows the shear stress calculated with Equation 27 for all the reservoir levels recorded during two years. Our results suggest that the calculated 20% maximum variation of the shear stress (*external factor*) is not enough to decrease the factor of safety of the landslide by 50%, which is the factor of safety reduction required in order for the landslide to admit its final collapse. This result is in agreement with previous studies on the landslide, like *Vardoulakis* [*2002*], *Alonso and Pinyol* [*2010*], and *Dykes and Bromhead* [*2018*]. Alternative mechanisms are therefore sought for destabilizing further the landslide, like the decrease of the friction coefficient (*internal factor*) or an increase of the pore water pressure (*internal factor*). A mechanism that is recently suggested for the latter, is the presence of perched aquifers inside the limestone strata and the propagation of cracks. These could increase abruptly the pore water pressure during periods of heavy rainfall for the Vaiont landslide [*Dykes and Bromhead, 2018*]. Although plausible, this hypothesis is impossible to be corroborated in the field [*Dykes and Bromhead, 2018a* page 1826] or by laboratory experiments. Other mechanisms described in the literature include various processes for frictional weakening, like thermal pressurization of the clay layers triggered by frictional heating [*Lachenbrunch, 1980*], strain and strain rate softening [*Tika and Hutchinson*, *1999*; *Vardoulakis, 2002*], or thermal softening [*Veveakis et al, 2007, Veveakis et al, 2010*]. Each of them could induce a reduction of the frictional resistance of the slide by 50%. Since the effects of strain, strain rate and temperature on the friction coefficient have been tested and validated by laboratory experiments [*Tika and Hutchinson*, *1999; Veveakis et al, 2010*], in this study we will focus on the combined effects of temperature and strain rate (velocity) on the shear strength of the clay layers as (internal) mechanisms to decrease the apparent factor of safety.

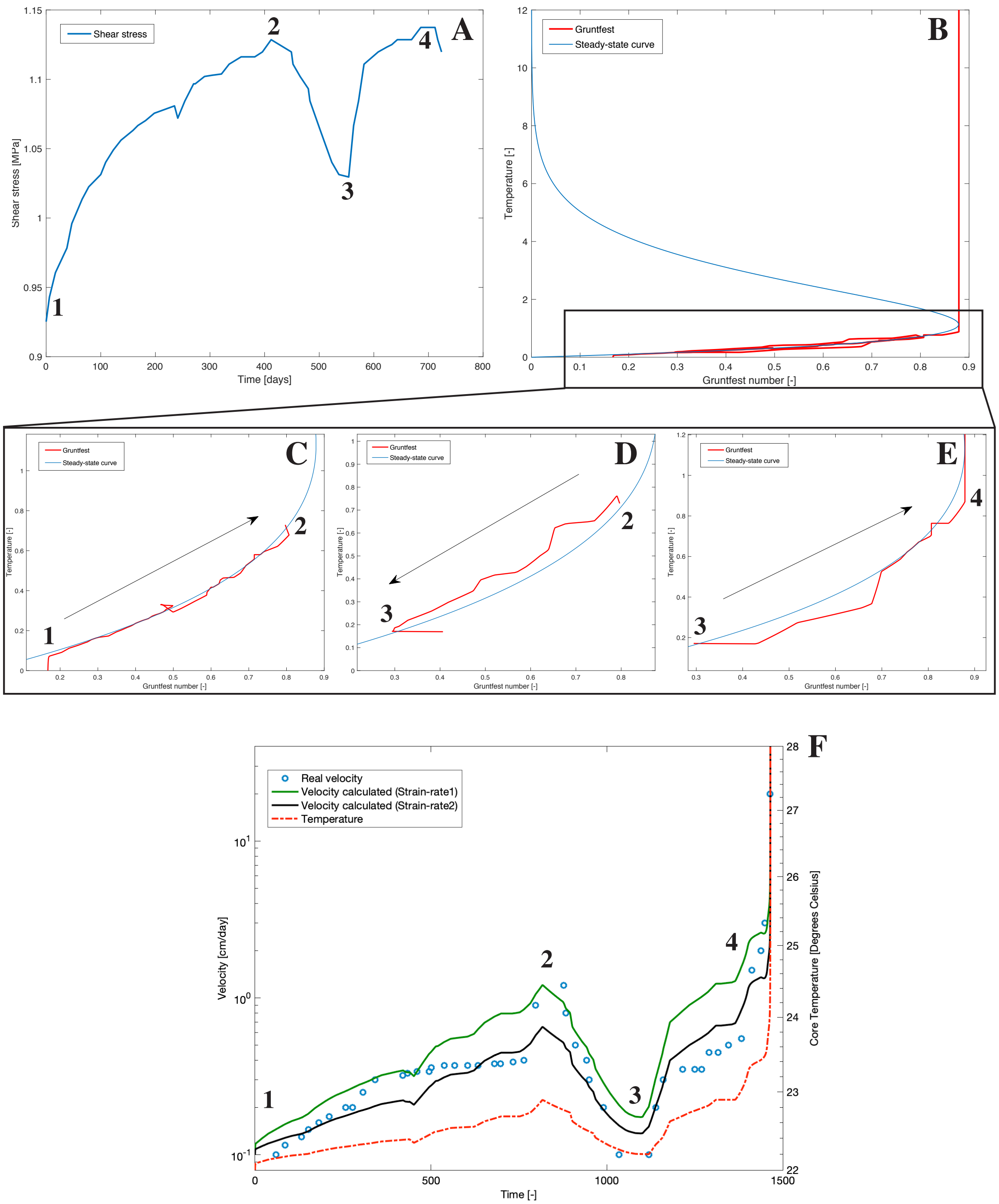

Figure 5. Results of the Vaiont slide: **A)** Graph that represents the shear stress value at each lake water level during the last two years of recorded data of the Vaiont dam. **B)** Gruntfest number calculated versus temperature, with the stability curve. **C)** Zoom of Figure 5B: Gruntfest number versus temperature for the first embankment of the reservoir, points 1 to 2 from Figure 5A. **D)** Zoom of Figure 5B: Gruntfest number versus temperature for the first reduction of the reservoir, points 2 to 3 from Figure 5A**. E)** Zoom of Figure 5B: Gruntfest number versus temperature for the second and last embankment of the reservoir, points 3 to 4 from Figure 5A. **F)** Velocity data from the field [*Müller, 1964*] as blue dots, two velocities calculated through

Equation (17) –keeping in mind that $\dot{\gamma} = \frac{\partial V}{\partial y}$ - as green and black lines, and red dashed/dotted line as a temperature in the shear band.

4.4 Transient stability analysis

In order to calculate the velocity of the landslide and the Gruntfest number, the material parameters of the clay that forms the shear band of Vaiont needed are retrieved from *Veveakis et al, 2007* (summarized also in Table 1).

In the case study of the Vaiont landslide, the mathematical system calculated becomes unstable for a value of the Gruntfest number of 0.88 and a value of the dimensionless temperature of 1.2 (Figure 5B). We can then fit the velocity obtained from the model against the field data described in *Müller, 1964*. In order to fit the real velocity taken from the field with the one calculated from our model, we adjust the velocity calculated with two limiting values of the reference strain-rate ($\dot{\gamma}_{0_1}$and $\dot{\gamma}_{0_2}$), thus, obtaining as a result 2 different velocities (Figure 5F). This exercise serves as an uncertainty quantification, providing a range of confidence for the least constrained parameters like the reference strain-rate.

As shown in Figures 4E and 5F, during the period of 2 years of data before the collapse of the landslide, the reservoir underwent two large fillings that affects significantly the outcome of the model in terms of shear stress, temperature in the shear band, and velocity. The fluctuations of the reservoir were performed in order to stabilize the landslide. When the landslide started to accelerate the reservoir level was decreased in order to stop its motion. However, when they performed the last decrease of the reservoir, they could not stop the acceleration of the sliding mass as the system had already outreached the stability line. The values of the shear stress (i.e. Gruntfest number) and the temperature in the shear band were already too large (Figure 5B), making it impossible to stop the landslide.

In Figure 5, we observe a critical temperature inside the shear band of 23.5°C. During the first filling of the reservoir, we can see that the landslide did not collapse because the temperature in the shear band (22.9°C) did not overcome the critical temperature. However, during the second embankment (Figure 5A), the temperature at the shear band had already overcome the critical temperature, resulting in a blowup (collapse of the landslide) despite the last discharge of the reservoir.

Table 1. Material parameters of the gouge of Vaiont [*Veveakis et al, 2007*] and Shuping landslides [*Li, 2015*; *Veveakis et al, 2007*].

	Vaiont	**Shuping**	
Parameter	**Value**	**Value**	**Units**
m	56.62	0.6	$°C^{-1}$
ds	0.161	0.7	m
k_m	$1.6\cdot10^{-7}$	$1.6\cdot10^{-7}$	m^2/s
jk_m	0.45	0.45	$J\ (°C\ m\ s)^{-1}$
$\dot{\gamma}_{0_1}$	$3.34\cdot10^{-2}$	$50.59\cdot10^{-2}$	s^{-1}
$\dot{\gamma}_{0_2}$	$6.28\cdot10^{-2}$	$44.95\cdot10^{-2}$	s^{-1}
N	0.01	1	[-]
M	0.56	12	[-]
θ_1	22	-	°C
D	-	10	m^2/s

5 Case study: Shuping landslide

The Shuping landslide (Figure 6B) is also an ancient landslide that was reactivated when the Three Gorges dam was constructed in June of 2003 and the artificial lake started filling up. The area around the dam is composed mainly of sandy mudstone and muddy sandstone from the Triassic Badong formation, and because of this lithology, several landslides were triggered. This area is subject to long periods of rainfall which is also at the origin of the reactivation of the landslides. This slide has a thickness between 30 and 70 meters and presents a total rock mass of 2.7×10^7 m^3 (Figure 6C). In this case, observations have shown that the landslide accelerates when the lake water level is decreased and remains stable when the reservoir level rises (Figure 6D). Thus, it has the opposite behavior from the Vaiont landslide, which accelerates when the reservoir increases. This main difference for the behaviors of the two landslides can be traced to the permeability of the sliding mass, as Vaiont has a high permeability and Shuping low permeability. Nonetheless, the behavior of the Shuping landslide and its possible causes will be explained in more detail in the following sections.

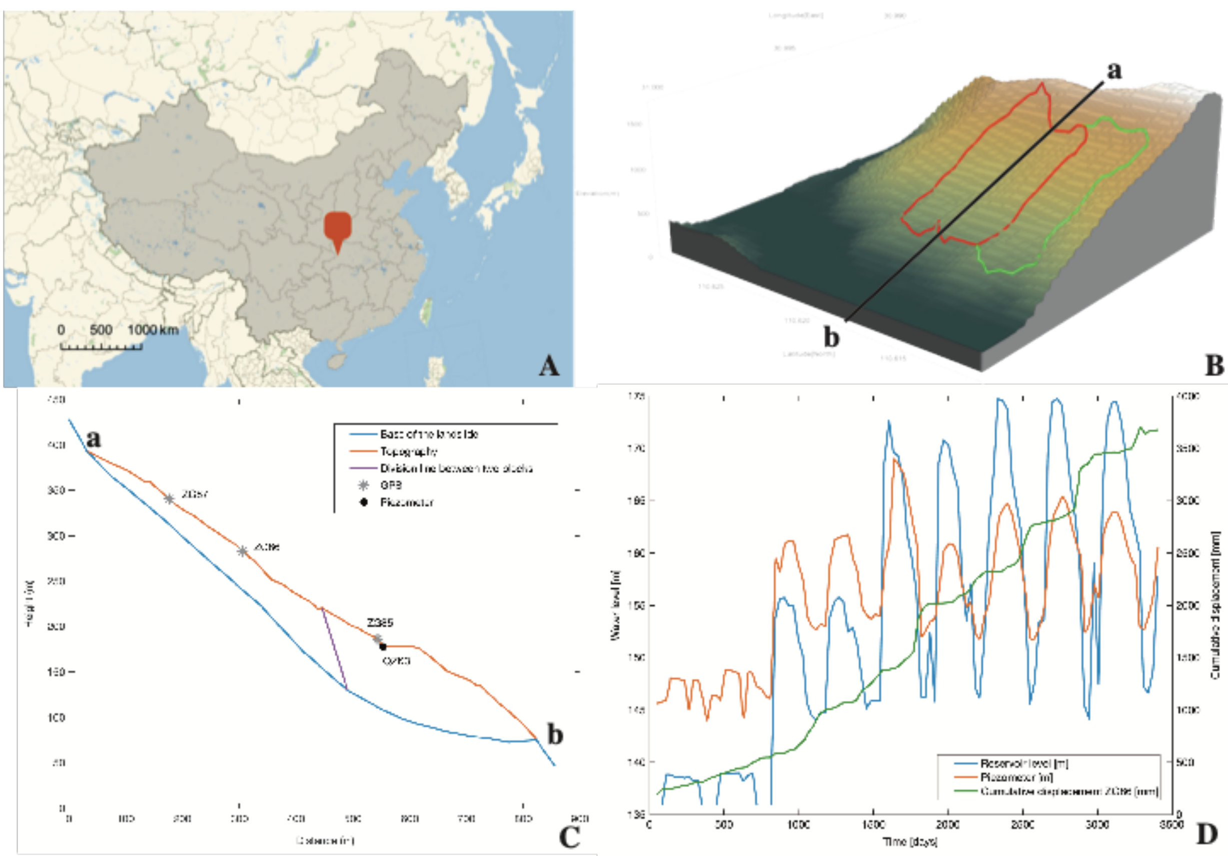

Figure 6. A) Map of location of the Shuping slide. **B)** 3D elevation map of the Shuping landslide (red is the active sector of the landslide and green is the dormant sector of the landslide). **C)** Profile of the deep-seated Shuping landslide. **D)** Graph showing the variations of the reservoir level, the variations of the groundwater level from the piezometer QZK3, and the displacement from the GPS ZG86 during the 10 years of recorded data [*Yin et al, 2016*].

5.1 Geographical location and geological framework

The Shuping landslide is located nearby the village of Xietanxiang, in Zigui county in Eastern China. The slide lies on the south crest of the valley where the Yangtze river flows along. Downstream the Yangtze river, at approximately 47km there is the Three Gorges Dam (Figure 6A).

The landslide is situated in the Southern part of the Shazhenxi anticline formed by mudstone, siltstone, and muddy limestone from the Triassic Badong formation. The layers of this formation in the south side of the anticline are dipping with an angle between 9 and 38° toward the direction of 120-173°. The top part of the landslide is formed by gravel, and the bottom part of the landslide is formed by clay and silty clay. The mass is sliding over a thin layer (0.6-1 m) of brown breccia soil and silty clay. And the underlying material of the landslide is composed by siltstone mixed with mudstone.

5.2 Groundwater analysis

To calculate the groundwater table for this case we used the transient method (Section 2.1) adding a diffusivity parameter (Equation 1) to fit the time lap that exists in the data between the variation of groundwater level and the displacement of the landslide (Figure 6D) [*Li, 2015*]. The boundary conditions chosen for this calculation have been the lake water level and the piezometer data that measured the groundwater level at QZK3 (see Figure 6C for location, *Wu et al, [2018]*).

As can be seen in Figure 6D, the groundwater level at the piezometer (QZK3) versus the lake water level is not constant (meaning that the piezometer level is not always above the lake level like in the case of the Vaiont landslide). Therefore, in Figure 7A and 7B can be seen the groundwater profile for a low lake water level and for a high lake water level, respectively.

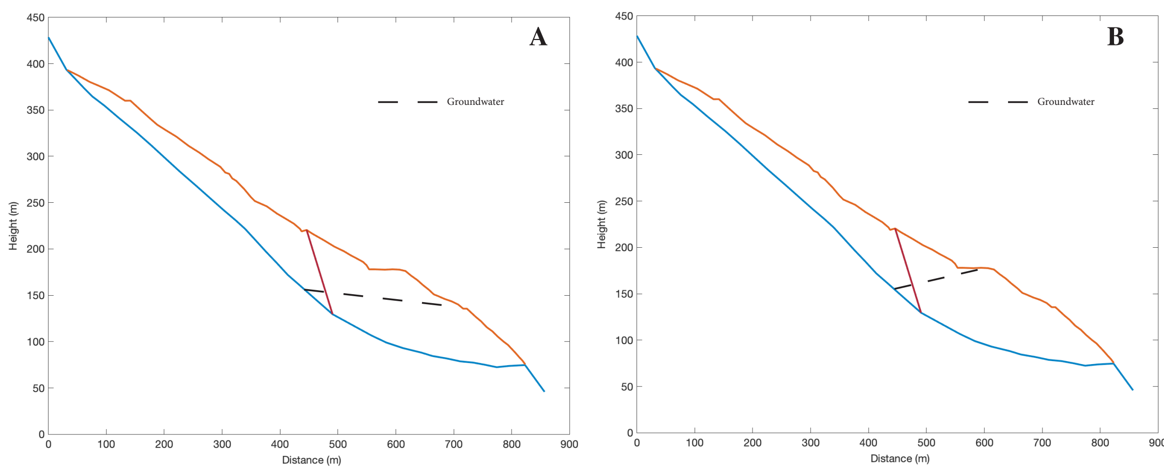

Figure 7. Profile of the Shuping landslide: **A)** Groundwater table when the reservoir level is at 135m. **B)** Groundwater table when the reservoir level is at 175m.

5.3 Shear stress results

In the case of Shuping landslide, we have enough data to straightforwardly calculate the shear stress for each lake level, without having to overestimate the basal shear stress value. In Figure 8A we plot the results of the shear stress calculated at each reservoir level for each period of time. The shear stress of the landslide varies between 1.12 and 1.2 MPa.

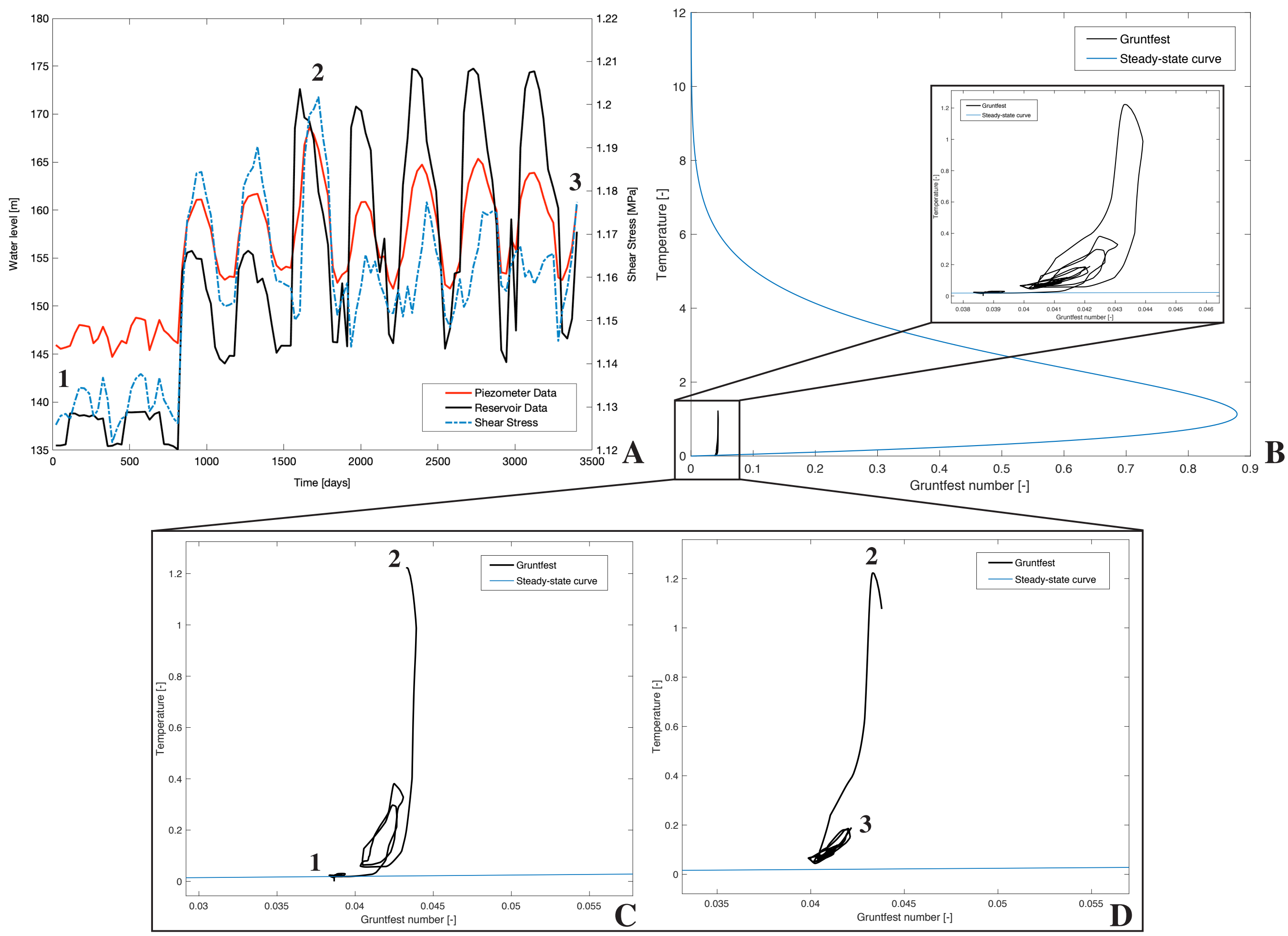

Figure 8. A) Graph showing the reservoir level, the piezometer data and the shear stress calculated for Shuping slide. **B)** Gruntfest number calculated versus temperature, with the steady-state curve. **C)** Zoom of Figure 8B: Gruntfest number versus temperature for the first behavior of the landslide, points 1 to 2 from Figure 8A. **D)** Zoom of Figure 8B: Gruntfest number versus temperature for the second behavior of the landslide, points 2 to 3 from Figure 8A**.**

5.4 Transient stability analysis

In order to calculate the velocity of the landslide and the Gruntfest number, we need the material parameters of the clay that form the shear band of the Shuping landslide (Table 1). Some of these parameters have been taken from the Vaiont landslide [*Veveakis et al., 2007*] due to the absence of further information and the fact that the shear band of Shuping is formed by similar clays as in Vaiont. The rest of the parameters were taken from *Li* [*2005*].

In this case study, the mathematical system calculated becomes unstable for a Gruntfest number of 0.88 and for a dimensionless ratio of temperature of 1.13 (Figure 8B). The value of the Gruntfest number for the case of Shuping is very simmilar to Vaiont, because we have assumed the same values of thermal conductivity. The shear stress is also very similar in magnitude as in Vaiont

To calculate the velocity, we have chosen the GPS data from the station ZG86 (Figure 6C) because this station represents well the average displacement (i.e. displacement of the center of mass) of the landslide, as the upper station ZG87 (Figure 6C) is located in an area that has been experiencing small localized slides. The same is true for the station ZG85 (Figure 6C), located below ZG86. While fitting the velocity calculated with the data of the ZG86 station, we also provided a confidence area bounded by two values of reference strain-rate ($\dot{\gamma}_{0_1}$and $\dot{\gamma}_{0_2}$, see Table 1), thus having with two velocity curves delimiting our parameter range (Figure 9A), as was also the case in the Vaiont slide.

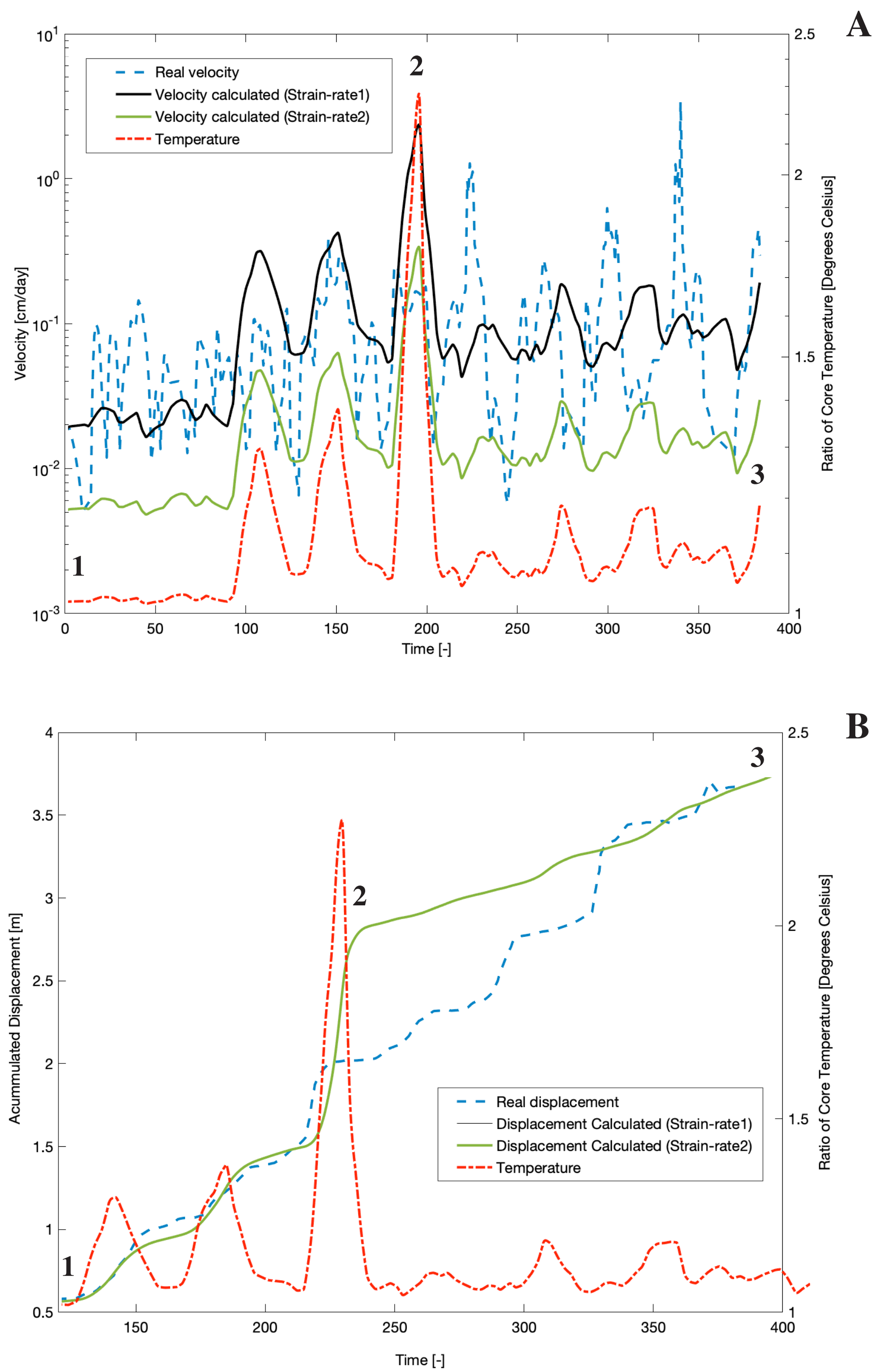

Figure 9. A) Velocity data from the field (calculated from the displacement obtained from [*Wu et al, 2018*]) as dashed line, two velocities calculated as lines, and dashed/dotted line indicating the ratio of the real temperature with the reference temperature in the shear band**. B)** Comparison of calculated displacement, ZG86 station displacement (blue dashed line), and ratio of the reference temperature and the real temperature (dashed/dotted line) in the shear band of Shuping landslide.

The calculated temperature shown in Figure 9A is the ratio of the real temperature in the shear band over the reference temperature. Therefore, if we have a reference temperature from the field, we can obtain the real temperature in the shear band at any groundwater level (thus, reservoir and piezometer levels). Once the velocity is calculated, we convert our results to displacement and compare it to the displacement data from the field (Figure 9B) and to the temperature calculated in the shear band in order to understand the behavior of the gouge that causes the instability of the landslide.

The two different reference strain-rates ($\dot{\boldsymbol{\gamma}}_{\mathbf{0}_\mathbf{1}}$and $\dot{\boldsymbol{\gamma}}_{\mathbf{0}_\mathbf{2}}$) applied to the calculations of velocity have been applied also to the displacements. Nevertheless, as Figure 9B shows, the different values of strain rate in the displacement do not affect the results of displacement. As it can be seen in Figure 9B, the model fits well the real data for the points 1 to 2, after that (points 2 to 3), the displacement increases smoother, due to the general behavior of the reservoir. This behavior is well represented in the shear stresses calculated (Figure 8A) and in the temperature of the gouge (Figure 9A) due to the fact that the three first cycles of the reservoir filling are sharper in terms of the shear stress due to the loads of the groundwater level in the landslide. After these three reservoir fillings, the shear stress varies in a smoother way. It can therefore be seen that the results of the applied model are consistent with the data and fit well the field data, taking into account that we are fitting 10 years of very irregular data. Furthermore, the results show that the behavior of the landslide (high displacements) is consistent with the temperature in the shear band and the shear stresses calculated.

Note on the inversion procedure: In the model implemented in this study, the rate sensitivity parameter N of the friction coefficient was modified in order to fit the velocity/displacement variations of the measured data. Once this parameter was determined, we adjusted the ratio of thermal and rate sensitivity coefficients m to calculate the Gruntfest number (i.e. the shear stresses) for the stability of the landslide. In the case of Vaiont, we know that the landslide collapses after the last embankment of the reservoir, thus the Gruntfest number crosses the steady state curve making the system become unstable. However, for the Shuping landslide, the instability point is uncertain as the landslide has not collapsed. Thus, we had chosen a value of N that fits as close as possible the real data (i.e. displacement), and the maximum value of m that keeps the system stable (as a larger value of m will change the system to unstable). Due to the previous facts, it is necessary to perform laboratory test of the clays located in the shear band of the Shuping landslide to get more information about the thermal sensitivity of these clays, thus we could get a better approximation of the critical Gr number required for the landslide to become unstable.

5.5 The behavior of Shuping landslide explained through groundwater regimes

It can be seen in either Figure 6D or Figure 8A that the Shuping landslide admits two distinct behaviors over the 10 years of its motion; 1) a more unstable from point 1 to point 2

(Figure 9B, see the values of temperature of the shear band) where the shear stresses and velocities are larger because the groundwater table behaves as a steady state (Figure 8A). In this period, the piezometer level was kept above the reservoir level with both points increasing or decreasing simultaneously. During this first period the groundwater level was following variations of the lake level and the landslide was accelerating with increasing lake level; 2) a second, more stable mechanism from point 2 to point 3 (Figure 9B, see the values of temperature of the shear band) where the shear stresses (Figure 8A) and velocities (Figure 9A) are lower because the groundwater table (Figure 8A) behaves in a transient manner, not having enough time to equilibrate. In this phase the piezometer level is below the reservoir level and inverse seepage is induced. This means that the landslide accelerates with decreasing lake level. This second mechanism is represented in Figure 8A where the groundwater table has an opposite slope (Figure 7B) than for the first mechanism.

A possible cause of the transient behavior of the second phase, could be that when the reservoir level is above 158 meters, there is a shift of the water heights between the reservoir level and the piezometer data (see Figure 8A where the two curves of piezometer and reservoir levels cross at 158 meters approximately for each cycle of loading/unloading of the reservoir). As can be seen in the data (Figure 8A), the maximum average of the piezometer level is 163 meters. Even though the reservoir level is above this value, the piezometer level does not increase (except for the first big embankment – 20 meters - of the reservoir at Point 2 of Figure 8A, which was a sudden rise of both the reservoir and piezometer). This fact suggests that the landslide mass is fully saturated and at maximum water capacity, i.e. the permeability of the sliding mass is low. Thus, when the reservoir level increases, instead of increasing the piezometer data in a steady state behavior, it experiences transient flow and the groundwater table changes its slope, making the landslide more stable as the shear stress values are lower (Figure 8A) than when the landslide behaves at steady-state. Because of the previous facts, it seems that maintaining the reservoir level above 158 meters will cause the landslide to be stable.

6 Summary and Conclusions

The cases of Vaiont and Shuping landslides were studied in this paper. For both cases, the implementation of time-dependent shear stress in the thermal model presented in *Veveakis et al.* [*2007*], allowed to reproduce the history of velocities and displacements for the the Vaiont and Shuping slides, respectively. The model presented in this paper combines the two main mechanisms that govern the behavior of a slide: the weakening of friction at the base of the slide and the pore pressure (thus the shear stress) evolution due to groundwater table variations. The analysis of the Vaiont landslide revealed that indeed the point where the heat dissipation process starts localizing is a critical point of the landslide. While in the case of the Shuping landslide, we were able to determine a region of stability of the system. However, for the case of Shuping, additional information of the properties of the shear band material would be needed in order to obtain with more accuracy the instability point.

We have shown with the analysis applied in this paper, that taking into account the heat produced due to friction in the clayey gouge allows for a stability point of the landslide to be determined and calculated. This point was indeed confirmed to be able to explain the response of both landslides to the groundwater variations performed in both cases. This method proves that even for different behaviors of landslides in terms of groundwater level (steady-state and transient) the model is valid, and we are able to find the point where the landslide turns unstable and renders the arrest of the sliding mass impossible. The results of this study against two distinctly different case studies, together with the fundamental nature of the physical mechanisms assumed in the mathematical formulation, suggest that this approach could be deployed as a tool of early warning for deep-seated landslide collapse.

Acknowledgments

Most of the concepts presented in this work are the result of a close collaboration, mentorship and friendship of E. Veveakis with late Prof. I. Vardoulakis. An early version of these ideas was in place since early 2008, when E.V. and I.V. were working together on the Vaiont landslide. Because of his untimely passing in mid-2009, these ideas never materialized in a concrete scientific publication. The present work is seen to be the ripened fruit of these ideas, and is therefore full-heartedly dedicated to late Prof. Ioannis Vardoulakis, for his guidance and inspirational ideas.

References

Alevizos S., Poulet T. and Veveakis, E. (2014). Thermo-poro-mechanics of chemically active faults. 1: Theory and steady-state considerations, *J. Geophys. Res. Vol 119 (6), 4558-4582, doi: 10.1002/2013JB010070,*

Alonso, E., (1989). Análisis de la estabilidad de taludes. Casos simples. En Corominas, J. (editor), “Estabilidad de Taludes y Laderas Naturales”, Monografía n° 3, Sociedad Española de Geomorfología, pp. 97-118. (In Spanish)

Alonso, E., (1989). Métodos generales de equilibrio límite. En Corominas, J. (editor), “Estabilidad de Taludes y Laderas Naturales”, Monografía n° 3, Sociedad Española de Geomorfología, pp. 119-166. (In Spanish)

Alonso, E. E., Pinyol, N. M. (2010). Criteria for rapid sliding I. A review of Vaiont case, Engineering Geology, 114, 198-210.

Alonso, E. E., Zervos, A., and Pinyol, N. M. (2016). Thermo-poro-mechanical analysis of landslides: from creeping behaviour to catastrophic failure, Géotechnique, 66 (3), 202-219.

Anderson, D. L. (1980), An earthquake induced heat mechanism to explain the loss of strength of large rock and earth slides, in Proceedings of the International Conference on Engineering for Protection from Natural Disasters, pp. 569-580, John Wiley, New York.

Cecinato, F., Zervos, A. (2012). Influence of thermomechanics in the catastrophic collapse of planar landslides. Can. Geotech. J., 49, No. 2, 207-225.

Cecinato, F., Zervos, A., Veveakis, E. (2011). A thermo-mechanical model for the catastrophic collapse of large landslides, Int. J. Numer. Anal. Meth. Geomech., 35, 1507-1535.

Chan, T.F.C., Keller, H.B., 1991. Arc-length continuation and multi-grid techniques for nonlinear elliptic eigenvalue problems. SIAM J. Sci. Stat. Comput. 3 (2), 173-194.

Craig, R.F., 2004. Craig’s Soil Mechanics. Seventh edition. ISBN 0-203-49410-5.

Dykes, A.P., Bromhead, E.N. (2018a). The Vaiont landslide: re-assessment of the evidence leads to rejection of the consensus, Landslides, 15, 1815-1832.

Dykes, A.P., Bromhead, E.N. (2018b). New, simplified and improved interpretation of the Vaiont landslide mechanics, Landslides, 15, 2001-2015.

Ferri, F., Di Toro, G., Hirose, T., Han, R., Noda, H., Shimamoto, T., Quaresimin, M., De Rossi, N., (2011). Low- to high-velocity frictional properties of the clay-rich gouges from the slipping zone of the 1963 Vaiont slide, northern Italy. Journal of Geophysical Research, Vol. 116, B09208.

Goren, L., Aharonov, E. (2007). Long runout landslides: The role of frictional heating and hydraulic diffusivity. Geophys. Res. Lett., 34, No. L07301, 1-7.

Goren, L., Aharonov, E. (2009). On the stability of landslides: a thermo-poro-elastic approach. Earth Planetary Sci. Lett., 277, No. 3-4, 365-372.

Goren, L., Aharonov, E., Anders, M. H. (2010). The long runout of the Heart Mountain landslide: Heating, pressurization, and carbonate decomposition. J. Geophys. Res.: Solid Earth 115, No. 10B, 1-15.

Gruntfest, I. J., (1963). Thermal Feedback in Liquid Flow: Plane Shear at Constant Stress, Trans. Soc. Rheology, 7, 195-207.

Habib, P., (1967). Sur un mode de glissement des massifs rocheaux, C.R. Acad. Sci., 264, 151-153. (In French)

Helmstetter, A., Sornette, D., Grasso, J. R., Andersen, J. V., Gluzman, S., Pisarenko, P. (2004). Slider block friction model for landslides: Application to Vaiont and La Clapière landslides, J. Geophys. Res., 109, B02409.

Hendron, A.J., Patton, F.D. (1985). The Vaiont slide, a geotechnical analysis based on new geologic observations of the failure surface, Technical Report GL-85-5. Washington, DC, Department of the Army US Corps of Engineers.

Kilburn, R.J.C. and Petley, D.M., (2003). Forecasting giant, catastrophic slope collapse: lessons from Vajont, Northern Italy, Geomorphology, 54, 21-32.

Lachenbrunch, A. H. (1980). Frictional heating, fluid pressure and the resistance to fault motion. J. Geophys. Res. 85, 6097-6112.

Li, Y., (2015). Mechanism of Landslides around China's Three Gorges Dam. Master Thesis. University of Alberta, Department of Civil and Environmental Engineering.

Ma, J., Tang, H., Liu, X., Wen, T., Zhang, J., Tan, Q., Fan, Z. (2017). Probabilistic forecasting of landslide displacement accounting for epistemic uncertainty: a case study in the Three Gorges Reservoir area, China. Landslides. DOI 10.1007/s10346-017-0941-5.

Mase, C.W. and Smith L. (1984). Pore-fluid pressures and frictional heating on a fault surface, PAGEOPH, Vol. 122 (2-4), 583-607, doi: 10.1007/BF00874618.

Muller, L., (1964). The rock slide in the Vaiont valley, Felsmech. Ingenoirgeol., 2, 148-212.

Muller, L., (1968). New considerations on the Vaiont slide, Felsmech. Ingenoirgeol., 6, 1-91.

Petley, D.N., Mantovani, F., Bulmer, M.H., Zannoni, A., (2005). The use of surface monitoring data for the interpretation of landslide movement patterns. Geomorphology, 66, 133-147.

Pinyol, N. M., Alonso, E.E. (2010). Criteria for rapid sliding II. Thermo-hydro-mechanical and scale effects in Vaiont case, Engineering Geology, 114, 211-227.

Poulet T., Veveakis E., K. Regenauer-Lieb, D.A. Yuen, 2014. Thermo-Poro-Mechanics of chemically active creeping faults. 3: The role of Serpentinite in Episodic Tremor and Slip sequences, and transition to chaos, *J. Geophys. Res. Vol 119 (6), 4606-4625, doi: 10.1002/ 2014JB011004.*

Rice, J., (2006). Heating and weakening of faults during earthquake slip, J. Geophys. Res., 111, B05311, doi: 10.1029/200JB004006.

Saito, M. (1965). Forecasting the time of occurrence of a slope failure, Proceedings of the 6th international conference on soil mechanics and foundation engineering, Montreal, Canada, Vol. 2, pp. 315-318.

Saito, M. (1969). Forecasting time of slope failure by tertiary creep, Proceedings of the 7th international conference on soil mechanics and foundation engineering, Mexico City, Mexico, Vol. 2, pp. 677-683.

Semenza, E. and Melidoro, E. (1992). Proceedings of the meeting on the 1963 Vaiont landslide. IAEG Italian Section and Dip Sci Geologiche e Paleontologiche, University of Ferrara, Publ 1, pp 1-218.

Song, K., Yan, E., Zhang, G., Yi, Q. (2014). Back analysis of hydraulic properties for a landslide in the Three Gorges Area. Conference paper in Geotechnical Special Publication, June 2014.

Sornette, D., Helmstetter, A., Andersen, J. V., Gluzman, S., Grasso, J. R., Pisarenko, V. (2004). Towards landslide predictions: Two case studies, Physica A, 338 (3-4), 605-632.

Tika, T.E., Hutchinson, J.N. (1999). Ring shear tests on soil from the Vaiont landslide slip surface, Géotechnique, 49, 59-74.

Vardoulakis, I., (2002a). Dynamic thermo-poro-mechanical Analysis of Catastrophic Landslides, Géotechnique, 52, 157-171.

Vardoulakis, I., (2002b). Steady shear and thermal run-away in clayey gouges, Int, J. Solids Struct., 39, 3831-3844.

Veveakis, E., Vardoulakis, I., and Di Toro, T., (2007). Thermoporomechanics of creeping landslides: The 1963 Vaiont slide, northern Italy. J. Geophys. Res., 112, F03026, doi: 10.1029/2006JF000702.

Veveakis, E., Alevizos, S., Vardoulakis, I., (2010). Chemical reaction capping of thermal instabilities during shear of frictional faults, Journal of the Mechanics and Physics of Solids, 58, 1175-1194.

Veveakis E., Poulet T. and Alevizos S, 2014. Thermo-poro-mechanics of chemically active faults. 2: Transient Considerations, *J. Geophys. Res. Vol 119 (6), 4583-4605 doi: 10.1002/2013JB010071.*

Veveakis, E. and Regenauer-Lieb, K., (2015). Cnoidal waves in solids, Journal of the Mechanics and Physics of Solids, 78, 231-248.

Voight, B. (1988). A method for prediction of volcanic eruptions, Nature, 332, 125-130.

Voight, B., and Faust, C., (1982). Frictional heat and strength loss in some rapid landslides, Géotechnique, 32, 43-54.

Wang, D. J., Tang, H-M, Zhang, Y-H, Li, C-D, Huang, L. (2017). An improved approach for evaluating the time-dependent stability of colluvial landslides during intense rainfall. Environ. Earth. Sci, 76:321.

Wu, Q., Tang, H., Ma, X., Wu, Y., Hu, X., Wang, L., Criss, R., Yuan, Y., Xu, Y., (2018). Identification of movement characteristics and casual factors of the Shuping landslide based on monitored displacements. Bulletin of Engineering Geology and the Environment. Doi:10.1007/s10064-018-1237-2.

Yin, Y., Huang, B., Wang, W., Wei, Y., Ma, X., Ma, F., (2016). Reservoir-induced landslides and risk control in Three Gorges Project on Yangtze River, China. Journal of Rock Mechanics and Geotechnical Engineering, 8, 577-595.

Yu, Z., Xu, G., Li, W. (2017). Deformation investigation and Stability Analysis of Large-scale controlled reservoir landslides in Badong County, Three Gorges Reservoir. Revista de la Facultad de Ingeniería U.C.V., Vol. 32, No. 16, pp. 655-668.

Zhao, Y., Li, Y., Zhang, L., Wang, Q. (2016). Groundwater level prediction of landslide based on classification and regression tree. Geodesy and Geodynamics, Vol. X, No. X, 1-8.